


UDC 528.94

ACCURACY ASSESSMENT OF THE EFFECT OF DIFFERENT FEATURE DESCRIPTORS ON THE AUTOMATIC CO-REGISTRATION OF OVERLAPPING IMAGES

Oluibukun Gbenga AJAYI¹, Ifeanyi Jonathan NWADIALOR²

¹Department of Land and Spatial Sciences, Namibia University of Science and Technology, Windhoek, Namibia

²Department of Surveying and Geoinformatics, Federal University of Technology, Minna, Nigeria

Article History:

- received 01 December 2022
- accepted 04 March 2024

Abstract. This research seeks to assess the effect of different selected feature descriptors on the accuracy of an automatic image registration scheme. Three different feature descriptors were selected based on their peculiar characteristics, and implemented in the process of developing the image registration scheme. These feature descriptors (Modified Harris and Stephens corner detector (MHCD), the Scale Invariant Feature Transform (SIFT) and the Speeded Up Robust Feature (SURF)) were used to automatically extract the conjugate points common to the overlapping image pairs used for the registration. Random Sampling Consensus (RANSAC) algorithm was used to exclude outliers and to fit the matched correspondences, Sum of Absolute Differences (SAD) which is a correlation-based feature matching metric was used for the feature match, while projective transformation function was used for the computation of the transformation matrix (T). The obtained overall result proved that the SURF algorithm outperforms the other two feature descriptors with an accuracy measure of -0.0009 pixels, while SIFT with a cumulative signed distance of 0.0328 pixels also proved to be more accurate than MHCD with a cumulative signed distance of 0.0457 pixels. The findings affirmed the importance of choosing the right feature descriptor in the overall accuracy of an automatic image registration scheme.

Keywords: image registration, data fusion, feature descriptors, digital image processing, remote sensing applications, mosaic generation.

 Corresponding author. E-mails: ogbajayi@gmail.com; oajayi@nust.na

1. Introduction

With the developments and advances in technology, photogrammetric, and remote sensing applications are fast gaining global acceptance in the geographical observation and monitoring of the earth surface (Tsai & Lin, 2017; Kleissl, 2013; Olaleye et al., 2015; Rittavee et al., 2009; Sindhu, 2014; Ting & Heng, 2016). These applications provide pictorial representations of an area and they give an overview of a geographical scene of interest in the form of images which afford the observer or image analyst the opportunity to acquire accurate spatial or geometric information about the sphere of interest. Since the images of a large area or object are often acquired in small patches depending on the sensor used for the image data acquisition, often, there is the need to fuse those patches into larger pictures for wider view. Also, images are visual models of the reality and unless they are registered onto the object, realistic measurements cannot be derived from them, hence, they must be mosaicked or

fused together in order to ensure holistic representation and enable stereoscopic view of the desired geographical area of interest (Olaleye et al., 2015). The process of fusing these image patches together is known as mosaicking or image-to-image registration (Ajayi, 2020).

Image registration is the process of registering an image to the object space (such as a map) or to another image (usually termed co-registration). It determines the relative orientation between two images. Given two different representations of the same object (or geographical scene), the aim of image co-registration is to find a transformation function which, when applied to one image, will align (or register) points in that image with their conjugate points in the other image of the same object (Calvin et al., 2019). The major issue in image registration is thus the task involved in finding the optimal or most efficient spatial and radiometric (intensity) transformation with specific emphasis on the spatial transformation. Establishing this spatial correspondence is a vital issue which arises in Digital Image Processing (DIP) especially when

pixel by pixel comparison is to be made on more than one image which represents the same scene (Xiaolong & Siamak, 1999; Zhang et al., 2014).

Though registration can be done by registering each image to the same map, direct image-to-image transformation is more common (co-registration). It is the process of establishing a spatial correspondence between two overlapping images such that the images' features on the image space correspond to their conjugate features in the object space (Xiaolong & Siamak, 1999), by determining the transformation that correlates the conjugate point in the two views of the overlapping image patches (Ajayi, 2014).

Generally, four (4) stages are involved in the registration of overlapping images. First, a decision has to be made on the type of primitive to be adopted. These primitives can be points, lines, or area/polygonal features. Once the primitive has been selected, correspondence or conjugate points must be established by devising a similarity measure, after which the mathematical relationship of the overlapping images will be established using a transformation function. This transformation can either be orthogonal, affine, or projective transformation functions. Finally, a controlling model that provides solution to the registration problem is implemented by the integration of these three stages (primitives, similarity measure, and transformation function) (Al-Ruzouq, 2004).

Different feature detection, description, extraction, and matching models have been developed and implemented in the development of an automatic image registration scheme (Tsai & Lin, 2017; Olaleye et al., 2015; Rittavee et al., 2009; Shih-Ming, 2012; Ting & Heng, 2016; Zhong et al., 2016). These models, together with other models used at every stage of image registration process, are of different characteristic features which make them suitable for different imaging conditions (Lin & Labuz, 2013; Lowe, 1999). The major characteristics of these models are summarized in Ajayi (2019) and Ajayi (2020). Also, Cuiyin et al. (2021) gave a systematic review of frequently used keypoints' detector and feature descriptors in image registration, including their characteristics, corresponding

principles and analysis. On the other hand, Guorong and Shuangming (2020) proposed a new feature descriptor for multimodal image registration by taking advantage of the illumination and contrast invariant properties of phase congruency to provide solution to the problem of non-linear changes between image pairs.

This research is aimed at investigating the effect of using different feature descriptor in extracting associated corresponding features used for the automatic registration of overlapping images. Three different feature detection and extraction algorithms were selected and implemented for the development of an automatic image registration scheme. These algorithms are: (1) The SURF algorithm (Bay et al., 2008), (2) The MHCD algorithm (Harris & Stephens, 1988), and (3) The SIFT algorithm (Lowe, 1999). The choice of these techniques was informed by their popular acceptance as they are regarded as the most implemented feature descriptors (Tsai & Lin, 2017) and they are known to be invariant to zoom, noise, scale, rotation and illumination (Krishna & Varghese, 2015). The three feature descriptors were individually used for the development of the automatic image registration scheme which was experimented in two different image registration campaigns using google earth images and images acquired with the aid of an Unmanned Aerial Vehicle (UAV).

2. Materials and methods

2.1. Data used for model experimentation

Two different image registration campaigns were adopted for the experimentation of the developed registration scheme using different overlapping image pairs. The first campaign seeks to evaluate the performance of the developed scheme with low resolution images while the second campaign was used to evaluate the performance of the developed scheme with high resolution images. The images used to test the performance level of the scheme in the first image registration campaign were extracted from google earth real-time online image data repository (see Figure 1a and 1b), showing part of the built-up area of the Federal University of Technology, Minna, Niger State,



a)



b)

Figure 1. Image data of part of FUTMinna, Main campus, Minna: a – base image; b – search image

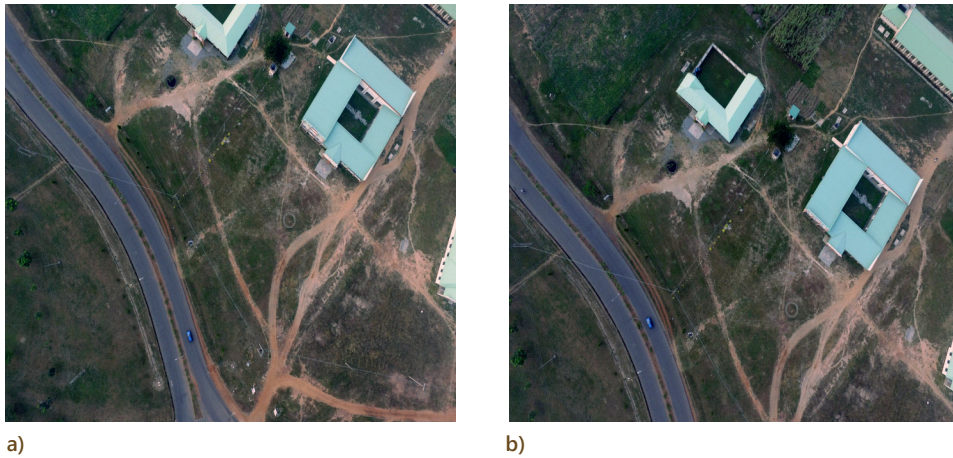


Figure 2. UAV acquired image of part of FUTMinna, Main Campus: a – base image; b – search image

Nigeria (Main Campus), while images acquired with the aid of a DJI Phantom 4 (Quadcopter) Unmanned Aerial Vehicle (UAV) covering part of the same campus, were used for the second image registration campaign (see Figure 2a and 2b).

Also, in order to ascertain the accuracy of the developed image registration scheme, coordinates of fifteen (15) ground control points (GCPs) distributed across the area covered by the overlapping image pairs were acquired with the aid of a handheld global positioning system (GPS) receiver. These GCPs are points that are identified on the overlapping image pairs as well as on the ground. Table 1 shows the coordinates of the 15 GCPs used for the first image registration campaign while the coordinates of the GCPs used for the second registration campaign is presented in Table 2.

Table 1. GCPs used for the first image registration campaign

STATION ID	Easting (m)	Northings (m)	Height (m)
FUTGK01	220 363.000	1 054 669.000	241.000
FUTGK02	220 394.000	1 054 704.000	241.000
FUTGK03	220 405.000	1 054 869.000	244.000
FUTGK04	220 528.000	1 054 702.000	240.000
FUTGK05	220 497.000	1 054 856.000	245.000
FUTGK06	220 514.000	1 054 940.000	245.000
FUTGK07	220 434.000	1 054 942.000	246.000
FUTGK08	220 427.000	1 055 042.000	243.000
FUTGK09	220 381.000	1 055 012.000	246.000
FUTGK10	220 368.000	1 055 190.000	243.000
FUTGK11	220 217.000	1 055 123.000	249.000
FUTGK12	220 203.000	1 054 920.000	256.000
FUTGK13	220 179.000	1 055 017.000	254.000
FUTGK14	220 144.000	1 055 077.000	251.000
FUTGK15	220 324.000	1 054 911.000	242.000

Table 2. GCPs used for the second image registration campaign

STATION ID	Easting (m)	Northing (m)	Height (m)
FUTGK-D-01	220 609.000	1 055 157.000	232.000
FUTGK-D-02	220 627.000	1 055 189.000	234.000
FUTGK-D-03	220 615.000	1 055 183.000	233.000
FUTGK-D-04	220 609.000	1 055 187.000	233.000
FUTGK-D-05	220 591.000	1 055 187.000	233.000
FUTGK-D-06	220 635.000	1 055 206.000	232.000
FUTGK-D-07	220 636.000	1 055 204.000	233.000
FUTGK-D-08	220 635.000	1 055 207.000	232.000
FUTGK-D-09	220 633.000	1 055 205.000	233.000
FUTGK-D-10	220 633.000	1 055 207.000	233.000
FUTGK-D-11	220 632.000	1 055 207.000	233.000
FUTGK-D-12	220 632.000	1 055 212.000	233.000
FUTGK-D-13	220 632.000	1 055 213.000	233.000
FUTGK-D-14	220 684.000	1 055 179.000	233.000
FUTGK-D-15	220 679.000	1 055 177.000	233.000

2.2. Model implementation and development of the image registration scheme

Feature based method of image registration which uses cost function as its similarity measure was adopted for the development of the image registration scheme.

The workflow of the automatic image registration paradigm adopted in this study consists of four (4) major stages. Figure 3 presents the algorithmic components of these four stages.

The implementation of these four basic stages involved in automatic image registration requires that they are subdivided into simpler steps. The process flow diagram for the feature-based registration algorithm is presented in Figure 4.

The details of the step-by-step procedure of implementing each of the three (3) feature detection and extraction algorithms, including their algorithmic activity diagrams, are presented in Ajayi (2020).

Having successfully detected and extracted the corresponding feature points automatically, which is inclusive of both inlier and outliers, the outliers which are the incorrectly matched points were filtered out using the Random

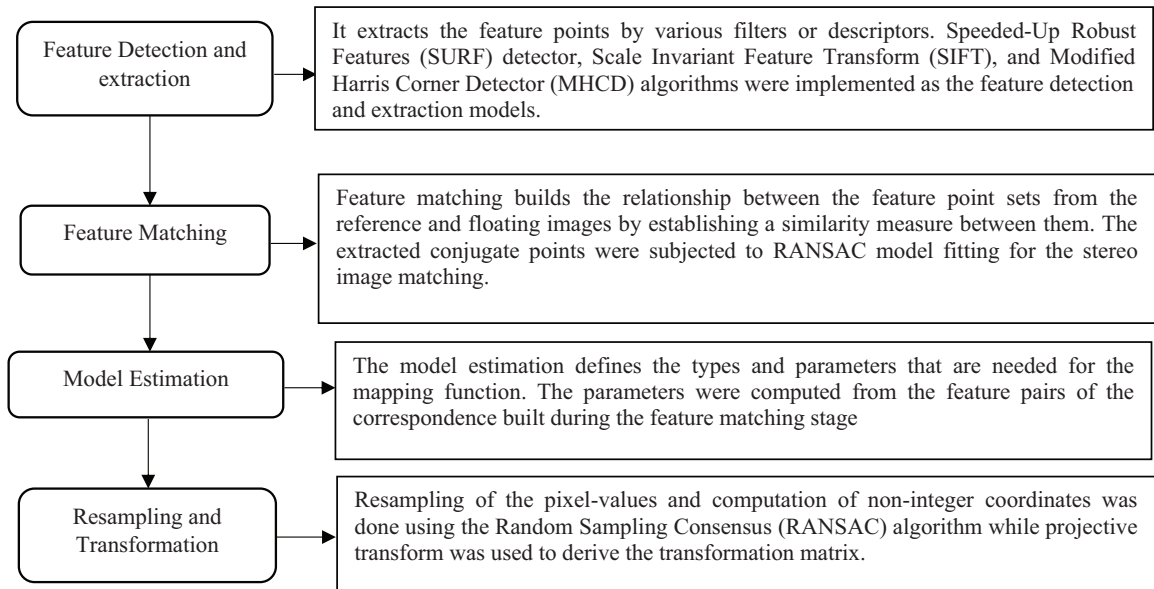


Figure 3. Process flow scheme of the basic stages of the automatic image registration model

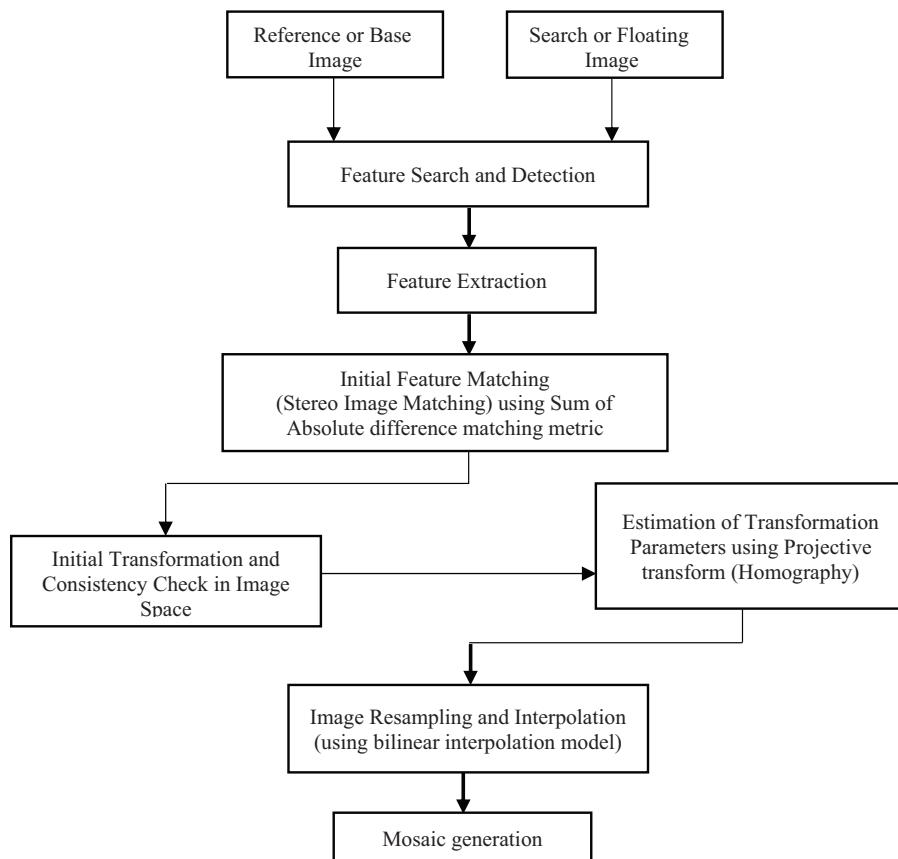


Figure 4. Flow diagram of the feature-based image co-registration scheme

Sampling Consensus (RANSAC) algorithm which was also used to fit the matched correspondences. The algorithmic procedure of implementing RANSAC is presented in Figure 5.

The Sum of Absolute Differences (SAD) which is a correlation-based feature matching method was used to build a relationship between the feature point sets from the reference and floating images because of its proven robustness (Scharstein & Szeliski, 2002). SAD is one of the simplest of all similarity measures and it is computed by the subtraction of pixels within a square neighbourhood between the reference image and the floating image, after which the absolute differences within the square window is aggregated before proceeding with the optimization using the winner-take-all (WTA) strategy (Kanade et al., 1997; Olaleye et al., 2015). In the event that the reference and floating images are perfectly matched, zero will be turned in as the resultant.

Bilinear interpolation algorithm which is a non-adaptive interpolation algorithm was implemented for the development of the automatic image registration scheme because it strikes the best balance between accuracy and computational complexity which makes it one of the most widely used interpolation algorithms. It uses the average weight of two-pixel values that has been translated and follows a computational procedure of first zero-padding the input matrix and translating it by the designated pixel value along the selected direction before creating the output matrix. The activity diagram describing the workflow of implementing the bilinear interpolation algorithm is presented in Figure 6.

Projective transformation function was used for the estimation of the transformation matrix. It is an eight-parameter (degrees of freedom) transformation, though with nine elements such as rotation, translation in X and Y directions, and perspective distortion in homogeneous coordinates. It preserves collinearity but does not preserve parallelism. It maps quadrangle onto a square and ensures that concurrency, collinearity, order of contact (tangency, inflection and intersection) and cross ratio are all invariant (Olaleye, 2010). It is the most suitable choice of transformation type when the transformation takes place between two planes (Al-Ruzouq, 2004), and hence was the adopted transformation function used in the development of the automatic image registration scheme presented in this study to ensure that the scheme can register multimodal image pairs.

Projective transformation allows the computation of the u, v coordinates of the points analytically after projecting them into a plane from another non-parallel plane which is expressed in Equation (1):

$$\phi \begin{bmatrix} a, b, c, d \\ e, f, g, h \end{bmatrix} \quad (1)$$

and can be written as Eqs (2)–(5):

$$\begin{bmatrix} x \\ y \end{bmatrix} = \frac{1}{t} \begin{bmatrix} a & b \\ d & e \end{bmatrix} \begin{bmatrix} u \\ v \end{bmatrix} + \frac{1}{t} \begin{bmatrix} c \\ f \end{bmatrix}, \quad (2)$$

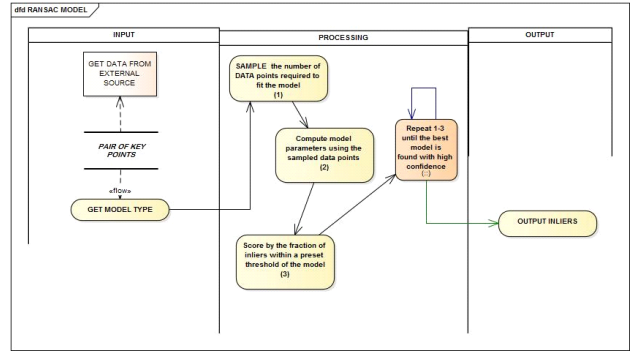


Figure 5. Activity diagram of Random Sampling Consensus (RANSAC) model

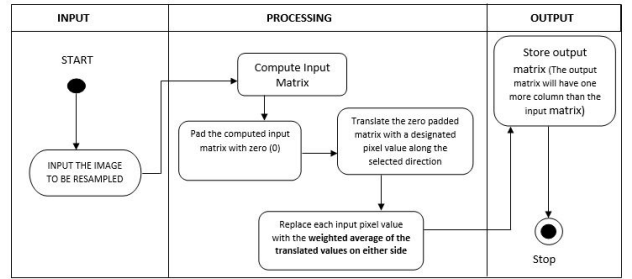


Figure 6. Activity diagram for the implementation of bilinear interpolation model

$$\text{where } t = gx + hy + 1; \quad (3)$$

$$x = \frac{ax + by + 1}{gx + hy + 1}; \quad (4)$$

$$\text{and } y = \frac{dx + cy + 1}{gx + hy + 1}. \quad (5)$$

Details of this transform are documented by Flusser (1994), Goshtasby (1988), and Goshtasby et al. (2003).

After developing the image registration scheme using JAVA programming codes, the scheme was experimented in two different image registration campaigns. The purpose of the first experiment is to examine the effect of the implemented feature descriptors on the overall accuracy of the developed image registration scheme when images of poor resolutions are used while the goal of the second objective is to assess the accuracy of the scheme when images of high resolutions are to be registered. Images extracted from google earth were degraded and used for the first campaign (Figure 1) while UAV acquired images were used for the second campaign as presented in Figure 2.

3. Results and discussion

The mosaics generated from the experimentation (first campaign) of the developed image registration scheme using MHCD, SIFT and SURF is presented in Figure 7a–c. In the registration scheme, each of the feature descriptors was individually used to automatically extract corresponding points or conjugate features on the overlapping image

pairs. The incorrectly matched points which are referred to as the outliers were excluded using RANSAC while the accurately matched points, known as inliers, were used for the estimation of the transformation matrix using projective transform and for the final registration.

A total of 456 conjugate points were automatically extracted using MHCD and the estimated transformation matrix of the image registration is

$$T_{Harris} = \begin{bmatrix} 1.00 & 0.00 & -243.836 \\ -0.00 & 1.00 & 1.887 \\ 0.00 & 0.00 & 0.99 \end{bmatrix}.$$

The transformation matrix shows that the diagonal is approximately equal to 1 and the parameter vectors of the computed homography are: $a = 1.000$, $b = 0.000$, $t_x = -243.836$ and $t_y = 1.887$. Where t_x and t_y are the translation along the x and y axis respectively, $a = \cos \alpha$ and $b = \sin \alpha$ while α is the rotation angle. For the SIFT model, a total of 1129 conjugate points were automatically and accurately extracted, and the estimated transformation matrix of the image registration is

$$T_{SIFT} = \begin{bmatrix} 1.00 & 0.00 & -243.967 \\ -0.00 & 1.00 & 2.061 \\ 0.00 & 0.00 & 1.00 \end{bmatrix}.$$

From the estimated transformation matrix, it was observed that the diagonal of the matrix is constant (with value 1.00) and the parameter vectors of the computed homography are: $a = 1.000$, $b = 0.000$, $t_x = -243.967$ and $t_y = 2.061$. Where t_x and t_y are the translation along the x and y axis respectively. Also, $a = \cos \alpha$, $b = \sin \alpha$ and α is the rotation angle. About 665 conjugate points were automatically extracted when SURF was used for the

automatic feature extraction and the estimated transformation matrix of the image registration is

$$T_{SURF} = \begin{bmatrix} 1.00 & 0.00 & -244.028 \\ -0.00 & 1.00 & 2.036 \\ 0.00 & 0.00 & 1.00 \end{bmatrix}.$$

From the estimated transformation matrix, it was observed that the diagonals of the matrix is constant (with values 1.00) and the parameter vectors of the computed homography are: $a = 1.000$, $b = 0.000$, $t_x = -244.028$ and $t_y = 2.036$. Where t_x and t_y are the translation along the x and y axis, respectively. Also, $a = \cos \alpha$, $b = \sin \alpha$ and α is the rotation angle.

From the parameter vectors of the transformation matrices generated when the three descriptors were used and the results of the three algorithms, it was discovered that the three feature descriptors proved to be indeed invariant to rotation as observed from the parameter vectors recorded in their estimated homography which shows a rotation angle that is equal to zero. This attests to the stability of the three algorithms, and this observation also agreed with the findings of Vivek and Kanchan (2014) and Panchal et al. (2013).

The cumulative signed distances of each of the point correspondences established automatically using MHCD, SIFT and SURF model were also estimated. The total signed distances of 0.0457 pixels, 0.0328 pixels, and -0.009 pixel were obtained as the residuals of the keypoints extracted using MHCD, SIFT and SURF, respectively. The obtained result also shows that SURF yielded a better accuracy when compared to SIFT and MHCD while SIFT also proved to be more accurate than MHCD. This is in tandem with the result obtained by Bolarinwa (2017).



a)



b)



Figure 7. Mosaic generated during the first campaign: a – using MHCD; b – using SIFT; c – using SURF model

3.1. Accuracy evaluation of the schemes using measured conjugate point data

The coordinates of the 15 GCPs presented in Table 1 were used for direct conjugate point measurements on the rectified images using the developed inbuilt stereo comparator of the image registration scheme. For the registration model using the three different feature detection and extraction algorithms, the coordinates of the GCPs were fed into the image registration scheme directly on the rectified image pair through the stereo comparator by identifying the GCPs on the image pairs. Once the data has been successfully entered, the stereo comparator automatically identifies and marks the conjugate points of the selected point on the other image pair (search image). Once all the points have been successfully measured, the developed registration scheme automatically generates a report which contains the image coordinates of each of the GCPs, computes the signed distances, and the root mean square error. This process was repeated for each of the three (3) feature detection and extraction algorithms used for the development of the image registration scheme.

Tables 3–5 presents the result obtained when the measurement was carried out on the rectified image using MHCD, SIFT and SURF, respectively. A signed distance of 0.0000 pixels was obtained from the direct point measurement using the three feature descriptors. Also, root mean square error of $6.6424709043813145 \times 10^{-14}$, $1.0407069005343235 \times 10^{-13}$, and $1.257834901735638 \times 10^{-13}$ were obtained when the MHCD, SIFT and SURF were used, respectively.

3.2. Automatic image registration using UAV acquired image pairs

For the second image registration campaign, the same methods adopted for the first image campaign were also used except for the overlapping image pairs and the GCPs used for the experimentation. Figure 8a–c presents the mosaic generated from the developed image registration scheme using the MHCD, SIFT and SURF feature descriptors on UAV images, respectively.

Using MHCD, a total of 172 conjugate points were automatically extracted and the estimated homography for the image registration is presented as:

$$H_{MHCD} = \begin{bmatrix} 1.001 & -0.005 & -74.022 \\ -0.009 & 1.024 & 583.624 \\ 0.000 & 0.000 & 0.976 \end{bmatrix}$$

The parameter vectors of the computed homography using MHCD in the second image registration campaign are: $a = 1.001$, $b = -0.005$, $t_x = -74.002$ and $t_y = 583.624$. Where t_x and t_y are the translation along the x and y axis respectively. Also, $a = \cos \alpha$, $b = \sin \alpha$ and α is the rotation angle. A total of 671 corresponding points were automatically matched and extracted when the SURF descriptor was used and the computed homography for the registration is given as:

$$H_{SURF} = \begin{bmatrix} 1.001 & -0.006 & -78.035 \\ -0.005 & 1.019 & 575.158 \\ 0.000 & 0.000 & 0.970 \end{bmatrix}$$

From the estimated homography, it was observed that the diagonals of the matrix is constant (1) and the

Table 3. Image locations of measured conjugate points and their signed distances (MHCD)

ID	Image location of conjugate points in Image A		Image location of conjugate points in Image B		Residuals
	x (Pixels)	y (Pixels)	x (Pixels)	y (Pixels)	Signed Distance (Pixels)
FUTGK01	326.135	325.812	82.166	327.861	0.000
FUTGK02	314.688	216.504	70.683	218.471	0.000
FUTGK03	280.135	149.717	36.075	151.602	0.000
FUTGK04	474.124	327.863	230.177	329.862	0.000
FUTGK05	526.639	599.599	282.622	601.422	0.000
FUTGK06	552.646	555.428	308.610	557.276	0.000
FUTGK07	564.883	384.318	320.880	386.275	0.000
FUTGK08	714.832	545.887	470.561	547.605	0.000
FUTGK09	652.870	406.136	408.771	408.038	0.000
FUTGK10	679.844	297.282	435.768	299.219	0.000
FUTGK11	594.855	299.049	350.857	301.009	0.000
FUTGK12	585.880	187.594	341.924	189.526	0.000
FUTGK13	535.137	225.283	291.189	227.237	0.000
FUTGK14	521.709	139.078	277.780	140.973	0.000
FUTGK15	356.931	100.207	112.932	102.032	0.000

parameter vectors of the computed homography are: $a = 1.001$, $b = -0.006$, $t_x = -78.035$ and $t_y = 575.158$. Where t_x and t_y are the translation along the x and y axis respectively. Also, $a = \cos \alpha$, $b = \sin \alpha$ and α is the rotation angle. Finally, a total of 1067 corresponding feature points were automatically extracted from the overlapping

image pairs when the SIFT descriptor was used and the estimated homography for the registration is given as:

$$H_{SIFT} = \begin{bmatrix} 1.001 & -0.005 & -72.334 \\ -0.008 & 1.023 & 582.473 \\ 0.000 & 0.000 & 0.976 \end{bmatrix}$$

Table 4. Image locations of measured conjugate points and their signed distances (SIFT)

ID	Image location of conjugate points in Image A		Image location of conjugate points in Image B		Residuals
	x (Pixels)	y (Pixels)	x (Pixels)	y (Pixels)	Signed Distances (Pixels)
FUTGK01	526.183	597.188	282.138	599.086	0.000
FUTGK02	552.381	555.668	308.344	557.591	0.000
FUTGK03	563.213	380.676	319.225	382.679	0.000
FUTGK04	714.255	547.080	470.202	549.003	0.000
FUTGK05	653.132	404.135	409.137	406.126	0.000
FUTGK06	680.407	297.590	436.452	299.609	0.000
FUTGK07	592.279	296.984	348.318	299.007	0.000
FUTGK08	585.753	187.575	341.825	189.611	0.000
FUTGK09	535.371	224.975	291.425	227.011	0.000
FUTGK10	521.672	139.628	277.746	141.666	0.000
FUTGK11	355.137	101.630	111.185	103.674	0.000
FUTGK12	329.406	323.265	85.424	325.294	0.000
FUTGK13	315.479	218.308	71.507	220.355	0.000
FUTGK14	279.242	149.997	35.271	152.048	0.000
FUTGK15	477.815	333.152	233.837	335.172	0.000

Table 5. Image locations of measured conjugate points and their signed distances (SURF)

ID	Image location of conjugate points in Image A		Image location of conjugate points in Image B		Residuals
	x (Pixels)	y (Pixels)	x (Pixels)	y (Pixels)	Signed Distances (Pixels)
FUTGK01	527.229	598.630	283.186	600.526	0.000
FUTGK02	552.077	556.071	308.024	557.976	0.000
FUTGK03	567.007	377.581	322.973	379.567	0.000
FUTGK04	711.639	547.453	467.428	549.256	0.000
FUTGK05	656.823	403.772	412.712	405.712	0.000
FUTGK06	678.203	296.363	434.098	298.352	0.000
FUTGK07	592.408	299.387	348.372	301.392	0.000
FUTGK08	583.953	188.307	339.942	190.332	0.000
FUTGK09	535.541	224.778	291.545	226.801	0.000
FUTGK10	525.013	138.359	281.031	140.379	0.000
FUTGK11	354.622	103.174	110.624	105.155	0.000
FUTGK12	327.824	324.663	83.820	326.722	0.000
FUTGK13	316.812	216.881	72.799	218.910	0.000
FUTGK14	279.457	151.241	35.417	153.237	0.000
FUTGK15	478.106	330.847	234.114	332.870	0.000



Figure 8. Mosaics generated for the UAV overlapping images using the three feature descriptors: a – using MHCD; b – using SIFT; c – using SURF

From the estimated homography, it was observed that the diagonal of the matrix is constant (with value 1.00) and the parameter vectors of the computed homography are: $a = 1.000$, $b = 0.000$, $t_x = -243.967$ and $t_y = 2.061$. Where t_x and t_y are the translation along the x and y axis respectively. Also, $a = \cos \alpha$, $b = \sin \alpha$ and α is the rotation angle.

From the results obtained in the second registration campaign, while there is no visual difference between the final mosaic generated using the three feature descriptors, there are marginal differences in their estimated transformation matrices. Based on the homography estimated for each of the implemented feature descriptors, it was observed that each of the feature descriptors proved to be invariant to rotation even when they were experimented with UAV acquired images. However, it was also noted that the SIFT descriptor was very robust in the automatic detection and extraction of corresponding features when compared to the MHCD and SURF descriptors. The SIFT algorithm automatically extracted conjugate points that are 1.59 times more than the conjugate points automatically extracted by SURF algorithm and 6.2 times more than the corresponding features automatically extracted by MHCD. This observation is also in agreement with the results obtained by Panchal et al. (2013) and Vivek and Kanchan (2014) which attests to the robustness of SIFT

in the automatic extraction of corresponding features or key points.

3.3. Performance evaluation of the developed scheme using UAV images

The two different approaches that were used for the evaluation of the first image registration campaign were also adopted for the second image registration campaign using UAV acquired overlapping image pairs. The first approach involves only the computation of the resultant signed distances of each of the automatically extracted point correspondences to evaluate the degree of mismatch while the RMSE and the cumulative signed distances obtained from the measured conjugate point data using the stereo-comparator were adopted as the second approach.

For the first approach, cumulative signed distance of 0.000 pixels, 0.000 pixels and 0.001 pixels were obtained from MHCD, SURF and SIFT algorithms, respectively, which shows perfect correlation for both MHCD and SURF, and near-perfect correlation for the SIFT descriptor.

Also, for the second performance evaluation approach, the GCPs presented in Table 2 were used to automatically locate conjugate points on the image pairs using the developed stereo-comparator. Tables 6–8

presents the photo coordinates of the measured conjugate points using the MHCD, SURF and SIFT, respectively. A cumulative signed distance of 0.000 was obtained for the three feature descriptors while RMSE of $5.74974632623059 \times 10^{-14}$, $1.153481152605981 \times 10^{-13}$, and $2.7426860557049027 \times 10^{-13}$ was estimated when the MHCD, SURF and SIFT algorithm were used, respectively.

4. Conclusions

This study presents the findings of the effect of selected feature descriptors on the overall accuracy of an automatic image registration scheme. Three different feature descriptors were selected and implemented for the development of the scheme. The obtained results showed that the choice of the feature descriptors affects the overall accuracy of

Table 6. Photo coordinates of measured conjugate points using MHCD (second image registration campaign)

ID	Image location of conjugate points in Image A		Image location of conjugate points in Image B		Residuals
	x (Pixels)	y (Pixels)	x (Pixels)	y (Pixels)	Signed Distance (Pixels)
FUTGK-D-01	2517.248	1552.172	2486.885	2192.373	0.000
FUTGK-D-02	3141.448	1282.213	3127.368	1906.770	0.000
FUTGK-D-03	2935.104	1176.964	2913.999	1819.004	0.000
FUTGK-D-04	2815.871	1078.300	2796.549	1699.187	0.000
FUTGK-D-05	3416.458	1120.877	3410.274	1736.076	0.000
FUTGK-D-06	3396.152	1104.729	3389.353	1721.007	0.000
FUTGK-D-07	3420.877	1069.581	3415.013	1684.166	0.000
FUTGK-D-08	3443.985	1087.671	3438.445	1702.776	0.000
FUTGK-D-09	3470.109	1054.104	3465.519	1667.566	0.000
FUTGK-D-10	3451.931	1034.994	3446.799	1649.411	0.000
FUTGK-D-11	3473.838	999.086	3469.584	1611.812	0.000
FUTGK-D-12	3496.692	1018.857	3492.737	1632.171	0.000
FUTGK-D-13	3828.283	2081.920	3821.378	2731.689	0.000
FUTGK-D-14	3813.617	2000.083	3806.914	2647.940	0.000
FUTGK-D-15	3875.180	1818.211	3870.772	2462.143	0.000

Table 7. Photo coordinates of measured conjugate points and their signed distances using SURF (second image registration campaign)

ID	Image location of conjugate points in Image A		Image location of conjugate points in Image B		Residuals
	x (Pixels)	y (Pixels)	x (Pixels)	y (Pixels)	Signed Distance (Pixels)
FUTGK-D-01	2517.161	1554.763	2487.033	2196.046	0.000
FUTGK-D-02	3139.986	1281.164	3124.857	1905.993	0.000
FUTGK-D-03	2926.008	1190.211	2905.228	1822.420	0.000
FUTGK-D-04	2782.964	1075.447	2763.109	1695.540	0.000
FUTGK-D-05	2609.824	879.176	2588.598	1493.103	0.000
FUTGK-D-06	3415.922	1121.928	3407.757	1738.040	0.000
FUTGK-D-07	3396.373	1104.191	3388.033	1719.793	0.000
FUTGK-D-08	3420.092	1069.979	3412.574	1684.036	0.000
FUTGK-D-09	3442.217	1086.367	3434.937	1700.858	0.000
FUTGK-D-10	3470.081	1052.479	3463.697	1665.400	0.000
FUTGK-D-11	3450.429	1034.387	3443.872	1646.784	0.000
FUTGK-D-12	3474.721	999.394	3468.328	1612.129	0.000
FUTGK-D-13	3493.780	1019.497	3487.521	1632.829	0.000
FUTGK-D-14	3827.696	2077.513	3817.169	2724.743	0.000
FUTGK-D-15	3804.463	1997.277	3794.421	2641.693	0.000

Table 8. Photo coordinates of measured conjugate points and their signed distances using SIFT (second image registration campaign)

ID	Image location of conjugate points in Image A		Image location of conjugate points in Image B		Residuals
	x (Pixels)	y (Pixels)	x (Pixels)	y (Pixels)	Signed Distance (Pixels)
FUTGK-D-01	2515.768	1554.831	2485.023	2196.245	0.000
FUTGK-D-02	3135.543	1281.555	3120.446	1906.336	0.000
FUTGK-D-03	2925.952	1189.691	2907.528	1813.009	0.000
FUTGK-D-04	2780.029	1074.980	2759.852	1695.320	0.000
FUTGK-D-05	2604.452	881.302	2582.768	1495.894	0.000
FUTGK-D-06	3414.916	1119.596	3407.474	1735.293	0.000
FUTGK-D-07	3394.461	1105.157	3386.751	1720.496	0.000
FUTGK-D-08	3420.435	1070.676	3413.659	1684.409	0.000
FUTGK-D-09	3445.664	1088.340	3439.223	1702.509	0.000
FUTGK-D-10	3448.713	1038.414	3442.898	1650.602	0.000
FUTGK-D-11	3472.279	1053.511	3466.793	1666.052	0.000
FUTGK-D-12	3473.939	999.646	3469.095	1610.063	0.000
FUTGK-D-13	3495.269	1020.655	3489.391	1634.594	0.000
FUTGK-D-14	3824.058	2081.935	3814.306	2730.720	0.000
FUTGK-D-15	3804.087	1997.551	3794.881	2643.308	0.000

the developed image registration scheme. Experimented over two different campaigns using google earth images and UAV acquired overlapping image pairs, the findings of the research showed that the SURF algorithm outperformed the SIFT and MHCD algorithms with a cumulative signed distance of 0.0009 pixels. On the other hand, SIFT algorithm proved to be more robust when compared with SURF algorithm and MHCD in terms of automatic extraction of corresponding features. It automatically extracted point correspondences which are approximately 2.5 times more than the point correspondences automatically extracted by the MHCD and 1.70 times more than the point correspondences automatically extracted by the SURF algorithm for the first image registration campaign. For the second registration campaign using UAV acquired image pairs, it automatically extracted conjugate points that are 1.59 times more than the conjugate points automatically extracted by SURF algorithm and 6.2 times more than the corresponding features automatically extracted by MHCD. This implies that the SURF algorithm is strongly recommended as the choice feature descriptor in the automatic image registration scheme when monomodal images are to be registered since only monomodal image pairs were experimented in this study over the two registration campaigns. The result also showed that the resolution of an image affects the number of corresponding features that can be extracted from it and also influences accuracy of the image registration. Further studies will experiment the performance of the developed registration scheme using these feature descriptors with multimodal images.

References

- Ajayi, O. G. (2014). *A MATLAB Program for the automatic registration of overlapping images* [MSc thesis]. Department of Surveying and Geoinformatics, Faculty of Engineering, University of Lagos, Nigeria.
- Ajayi, O. G. (2019). *Development of an integrated automatic image registration scheme* [PhD thesis]. Department of Surveying and Geoinformatics, School of Postgraduate Studies, Federal University of Technology, Minna, Nigeria.
- Ajayi, O. G. (2020). Performance analysis of selected feature descriptors used for automatic image registration. *The International Archives of the Photogrammetry, Remote Sensing and Spatial Information Sciences*, XLIII-B3-2020, 559–566. <https://doi.org/10.5194/isprs-archives-XLIII-B3-2020-559-2020>
- Al-Ruzouq, R. (2004). *Semi-Automatic registration of multisource satellite imagery with varying geometric resolutions* [PhD thesis]. Geomatics Engineering Department, Faculty of Graduate Studies, Calgary, Alberta.
- Bay, H., Ess, A., Tuytelaars, T., & Van, G. L. (2008). Speeded Up Robust Features (SURF). *Computer Vision and Image Understanding*, 110(3), 346–359. <https://doi.org/10.1016/j.cviu.2007.09.014>
- Bolarinwa, O. O. (2017). *Development of a semi-automated digital stereo comparator* [MSc thesis]. Department of Surveying and Geoinformatics, University of Lagos, Akoka-Lagos.
- Calvin, J. M., Gotsman, C. J., & Zheng, C. (2019). Global optimization for image registration. *AIP Conference Proceedings*, 2070, Article 020008. <https://doi.org/10.1063/1.5089975>
- Cuiyin, L., Jishang, X., & Feng, W. (2021). A review of keypoints' detection and feature description in image registration. *Scientific Programming*, 2021, Article 8509164. <https://doi.org/10.1155/2021/8509164>
- Flusser, J. (1994). A moment-based approach to registration of images with affine geometric distortion. *IEEE Transaction on*

- Geoscience and Remote Sensing*, 32(1), 382–387.
<https://doi.org/10.1109/36.295052>
- Goshtasby, A. (1988). Registration of images with geometric distortions. *IEEE Transactions on Geoscience and Remote Sensing*, 26, 60–64. <https://doi.org/10.1109/36.3000>
- Goshtasby, A., Lawrence, S., Studholme, C., & Terzopoulos, D. (2003). Non-rigid image registration: Guest editor's Introduction. *Computer Vision and Image Understanding*, 89, 109–113. [https://doi.org/10.1016/S1077-3142\(03\)00016-X](https://doi.org/10.1016/S1077-3142(03)00016-X)
- Guorong, Y., & Shuangming, Z. (2020). A new feature descriptor for multimodal image registration using phase congruency. *Sensors*, 20(18), Article 5105. <https://doi.org/10.3390/s20185105>
- Harris, C., & Stephens, M. (1988). A combined corner and edge detector. In *Proceedings of the 4th Alvey Vision Conference* (pp. 147–151). Alvey Vision Club. <https://doi.org/10.5244/C.2.23>
- Kanade, K., Jansa, J., & Kager, H. (1997). *Photogrammetry- advanced methods and applications*. Ferd. Dummlers Verlag.
- Kleissl, J. (2013). *Solar energy forecasting and resource assessment*. Academic Press.
- Krishna, S., & Varghese, A. (2015). Feature based automatic multiview image registration. *International Journal of Computer Science and Software Engineering*, 4(11), 308–314.
- Lin, Q., & Labuz, J. F. (2013). Fracture of sandstone characterized by digital image correlation. *International Journal of Rock Mechanics and Mining Sciences*, 60, 235–245. <https://doi.org/10.1016/j.ijrmms.2012.12.043>
- Lowe, D. G. (1999). Object recognition from local scale-invariant features. In *Proceedings of the International Conference on Computer Vision* (pp. 1150–1157). IEEE. <https://doi.org/10.1109/ICCV.1999.790410>
- Olaleye, J. B. (2010). *Mapping from images by vector photogrammetry*. [Unpublished Series in Geoinformatics, Lecture Note 10-1]. Dept. of Surveying and Geoinformatics, University of Lagos.
- Olaleye, J. B., Ajayi O. G., Omogunloye, O. G., Odumosu, J. O., & Okorocho, C. V. (2015). Automatic registration of simultaneously overlapping images. *NED University Journal of Research – Applied Sciences*, XII(4), 53–66.
- Panchal, P. M., Panchal, S. R., & Shah, S. K. (2013). A comparison of SIFT and SURF. *International Journal of Innovative Research in Computer and Communication Engineering*, 1(2), 323–327.
- Rittavee, M., Yuan, F. Z., & Robert, L. E. (2009). Image registration using adaptive polar transform. *IEEE Transaction on Image Processing*, 18(10), 2340–2354. <https://doi.org/10.1109/TIP.2009.2025010>
- Scharstein, D., & Szeliski, R. (2002). A taxonomy and evaluation of dense two-frame stereo correspondence algorithms. *International Journal of Computer Vision*, 47(1/2/3), 7–42. <https://doi.org/10.1023/A:1014573219977>
- Shih-Ming, J. (2012). Technique of image registration in digital image processing – A review. *International Journal of Information Technology and Knowledge Management*, 5(2), 239–243.
- Sindhu, M. G. (2014). Classification of image registration techniques and algorithms in digital image processing – a research survey. *International Journal of Computer Trends and Technology*, 15(2), 78–82. <https://doi.org/10.14445/22312803/IJCTT-V15P118>
- Ting, X. L., & Herng, H. C. (2016). Medical image registration based on an improved ant colony optimization Algorithm. *International Journal of Pharmacy, Medicine and Biological Sciences*, 5(1), 17–22.
- Tsai, C.-H., & Lin, Y.-C. (2017). An accelerated image matching technique for UAV orthoimage registration. *ISPRS Journal of Photogrammetry and Remote Sensing*, 128, 130–145. <https://doi.org/10.1016/j.isprsjprs.2017.03.017>
- Vivek, K. G., & Kanchan, C. (2014). An analytical study of SIFT and SURF in image registration. *International Journal of Engineering and Innovative Technology*, 3(9), 130–134.
- Xiaolong, D., & Siamak, K. (1999). A feature based image registration algorithm using improved chain-code representation combined with invariant moments. *IEEE Transactions on Geoscience and Remote Sensing*, 37(5), 2351–2362. <https://doi.org/10.1109/36.789634>
- Zhang, P. F., Li, X. Y., & Ma, L. (2014). Grid computing based on game optimization theory for networks scheduling. *Journal of Network and Computer Applications*, 9(5), 1295–1300. <https://doi.org/10.4304/jnw.9.5.1295-1300>
- Zhong, Z., Guo, X., Cai, Y., Yang, Y., Wang, J., Jia, X., & Mao, W. (2016). 3D-2D deformable image registration using feature based nonuniform meshes. *BioMed Research International*, 2016, Article 4382854. <https://doi.org/10.1155/2016/4382854>